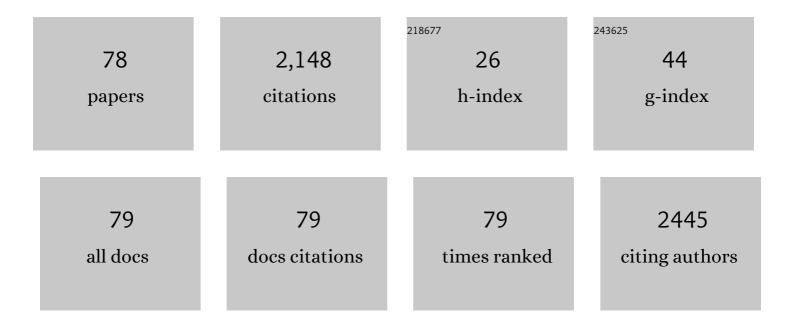
## Yuxuan Xie

List of Publications by Year in descending order

Source: https://exaly.com/author-pdf/1761088/publications.pdf Version: 2024-02-01



#	Article	IF	CITATIONS
1	Experimental observations of amorphization in multiple generations of boron carbide. Journal of the American Ceramic Society, 2022, 105, 3008-3029.	3.8	4
2	Addressing amorphization and transgranular fracture of B <sub>4</sub> C through Si doping and TiB <sub>2</sub> microparticle reinforcing. Journal of the American Ceramic Society, 2022, 105, 2959-2977.	3.8	11
3	Effect of crystallite geometries on electrochemical performance of porous intercalation electrodes by multiscale operando investigation. Nature Materials, 2022, 21, 217-227.	27.5	35
4	Twinning pathways enabled by precipitates in AZ91. Materialia, 2022, 21, 101292.	2.7	12
5	Effect of local twin Schmid factor on the tension twinning activities in a highly textured Mg–3Al–1Zn alloy under different strain paths. MRS Communications, 2022, 12, 217-222.	1.8	6
6	Decoupling the metal–insulator transition temperature and hysteresis of VO <sub>2</sub> using Ge alloying and oxygen vacancies. Chemical Communications, 2022, 58, 6586-6589.	4.1	6
7	Structure and substructure characterization of solution-treated Ni50.3Ti29.7Hf20 high-temperature shape memory alloy. Scripta Materialia, 2022, 219, 114888.	5.2	4
8	Understanding the interaction of extension twinning and basal-plate precipitates in Mg-9Al using precession electron diffraction. Materialia, 2021, 15, 101044.	2.7	15
9	Persistence of crystal orientations across sub-micron-scale "super-grains―in self-organized Cu-W nanocomposites. Scripta Materialia, 2021, 194, 113677.	5.2	4
10	Significant disparity of non-basal dislocation activities in hot-rolled highly-textured Mg and Mg-3Al-1Zn alloy under tension. Acta Materialia, 2021, 207, 116691.	7.9	41
11	Dislocation imaging via the virtual dark-field technique using the precession electron diffraction data. Microscopy and Microanalysis, 2021, 27, 2916-2917.	0.4	0
12	Exploring the origins of the indentation size effect at submicron scales. Proceedings of the National Academy of Sciences of the United States of America, 2021, 118, .	7.1	29
13	On the exceptionally high ductility of Mg–2Zn-0.3Ca-0.2Ce-0.1Mn alloy. Materials Science & Engineering A: Structural Materials: Properties, Microstructure and Processing, 2021, 819, 141484.	5.6	6
14	The mechanical behavior of single crystal and polycrystalline pure magnesium. Mechanics of Materials, 2021, 163, 104078.	3.2	2
15	Large areal capacity and dendrite-free anodes with long lifetime enabled by distributed lithium plating with mossy manganese oxides. Journal of Materials Chemistry A, 2021, 9, 9291-9300.	10.3	6
16	Twin boundary migration mechanisms in quasi-statically compressed and plate-impacted Mg single crystals. Science Advances, 2021, 7, eabg3443.	10.3	12
17	Mapping mechanisms and growth regimes of magnesium electrodeposition at high current densities. Materials Horizons, 2020, 7, 843-854.	12.2	77
18	Dislocation Imaging by Precession Electron Diffraction. Microscopy and Microanalysis, 2020, 26, 226-227.	0.4	1

#	Article	IF	CITATIONS
19	The Effect of Microstructure Morphology on Indentation Response of Ta/Ti Nanocomposite Thin Films. Metallurgical and Materials Transactions A: Physical Metallurgy and Materials Science, 2020, 51, 5677-5690.	2.2	5
20	Comparative study of helium bubbles in a Ti-Ta alloy and a Ti/Ta nanocomposite. Philosophical Magazine Letters, 2020, 100, 307-318.	1.2	1
21	Grain-subdivision-dominated microstructure evolution in shear bands at high rates. Materials Research Letters, 2020, 8, 328-334.	8.7	13
22	Understanding of Lithium Insertion into 3D Porous Carbon Scaffolds with Hybridized Lithiophobic and Lithiophilic Surfaces by In-Operando Study. Nano Letters, 2020, 20, 3681-3687.	9.1	20
23	Interface stability of laser powder-bed-fused AlSi12 under simulated atmospheric conditions. Corrosion Science, 2020, 175, 108861.	6.6	3
24	Non-dissociated <c+a> dislocations in an AZ31 alloy revealed by transmission electron microscopy. Materials Research Letters, 2020, 8, 145-150.</c+a>	8.7	8
25	The effect of boron and aluminum additions on the microstructure of arcâ€melted boron carbide. Journal of the American Ceramic Society, 2020, 103, 3453-3457.	3.8	3
26	Activation and suppression of ã€^cÂ+Âa〉 dislocations in a textured Mg–3Al–1Zn alloy. Scripta Materialia, 2020, 179, 49-54.	5.2	22
27	Damage relief of ion-irradiated Inconel alloy 718 via annealing. Nuclear Instruments & Methods in Physics Research B, 2020, 479, 157-162.	1.4	2
28	Revealing the Microstructural Information of the Quasi-Plastic Zone in a Boron Carbide Using the Advanced Precession Electron Diffraction Technique. Microscopy and Microanalysis, 2019, 25, 788-789.	0.4	1
29	Effect of temperature on the transition in deformation modes in Mg single crystals. Acta Materialia, 2019, 178, 241-248.	7.9	21
30	Experimental observations of the mechanisms associated with the high hardening and low strain to failure of magnesium. Materialia, 2019, 8, 100504.	2.7	13
31	Anomalous work hardening behavior of Fe40Mn40Cr10Co10 high entropy alloy single crystals deformed by twinning and slip. Acta Materialia, 2019, 181, 555-569.	7.9	72
32	High Moisture Barrier with Synergistic Combination of SiO <i><sub>x</sub></i> and Polyelectrolyte Nanolayers. Advanced Materials Interfaces, 2019, 6, 1900740.	3.7	10
33	Small amount TiB <sub>2</sub> addition into B <sub>4</sub> C through sputter deposition and hot pressing. Journal of the American Ceramic Society, 2019, 102, 4421-4426.	3.8	12
34	Molten salt synthesis of highly ordered and nanostructured hexagonal boron nitride. Diamond and Related Materials, 2019, 93, 179-186.	3.9	12
35	Tuning the deformation mechanisms of boron carbide via silicon doping. Science Advances, 2019, 5, eaay0352.	10.3	26
36	Formation of Magnesium Dendrites during Electrodeposition. ACS Energy Letters, 2019, 4, 375-376.	17.4	221

#	Article	IF	CITATIONS
37	Fabrication of dense B4C-preceramic polymer derived SiC composite. Journal of the European Ceramic Society, 2019, 39, 718-725.	5.7	17
38	Effect of synthesis conditions of BCNO on the formation and structural ordering of boron nitride at high temperatures. Journal of Solid State Chemistry, 2019, 269, 212-219.	2.9	10
39	Formation of metastable wurtzite phase boron nitride by emulsion detonation synthesis. Journal of the American Ceramic Society, 2018, 101, 3276-3281.	3.8	9
40	Nano-scale Elastic Strain Maps of Twins in Magnesium Alloys. Microscopy and Microanalysis, 2018, 24, 970-971.	0.4	7
41	Locating Si atoms in Si-doped boron carbide: A route to understand amorphization mitigation mechanism. Acta Materialia, 2018, 157, 106-113.	7.9	42
42	An etÂal. Reply:. Physical Review Letters, 2017, 118, 089602.	7.8	12
43	The effect of Si on the microstructure and mechanical properties of spark plasma sintered boron carbide. Materials Characterization, 2017, 134, 274-278.	4.4	31
44	Microstructural characterization of boron-rich boron carbide. Acta Materialia, 2017, 136, 202-214.	7.9	91
45	Nanotwinned metal MEMS films with unprecedented strength and stability. Science Advances, 2017, 3, e1700685.	10.3	68
46	Damage evolution of hot-pressed boron carbide under confined dynamic compression. International Journal of Impact Engineering, 2017, 99, 75-84.	5.0	33
47	New Ground-State Crystal Structure of Elemental Boron. Physical Review Letters, 2016, 117, 085501.	7.8	44
48	Breaking the icosahedra in boron carbide. Proceedings of the National Academy of Sciences of the United States of America, 2016, 113, 12012-12016.	7.1	31
49	Superstrength through Nanotwinning. Nano Letters, 2016, 16, 7573-7579.	9.1	62
50	Microstructural Characterization of a Commercial Hotâ€Pressed Boron Carbide Armor Plate. Journal of the American Ceramic Society, 2016, 99, 2834-2841.	3.8	36
51	Pyramidal I slip in c-axis compressed Mg single crystals. Scripta Materialia, 2016, 112, 75-78.	5.2	105
52	Deformation behavior of Mg single crystals compressed along c-axis. , 2016, , 209-211.		0
53	Atomic-Level Understanding of "Asymmetric Twins―in Boron Carbide. Physical Review Letters, 2015, 115, 175501.	7.8	56
54	Microstructural evolution of pure magnesium under high strain rate loading. Acta Materialia, 2015, 87, 56-67.	7.9	168

#	Article	IF	CITATIONS
55	Precipitation of AlN in a commercial hot-pressed boron carbide. Scripta Materialia, 2015, 101, 95-98.	5.2	12
56	Effect of Alumina on the Structure and Mechanical Properties of Spark Plasma Sintered Boron Carbide. Journal of the American Ceramic Society, 2014, 97, 3710-3718.	3.8	36
57	Ultrahigh-strength submicron-sized metallic glass wires. Scripta Materialia, 2014, 84-85, 27-30.	5.2	17
58	Resolving the Morphology of Niobium Carbonitride Nano-Precipitates in Steel Using Atom Probe Tomography. Microscopy and Microanalysis, 2014, 20, 1100-1110.	0.4	30
59	The mechanical behaviour of TiN and multi-layered coating of TiN/Ti on Ti6Al4V substrate during nano-indentation. International Journal of Surface Science and Engineering, 2014, 8, 95.	0.4	4
60	Nanocrystalline β-Ti alloy with high hardness, low Young's modulus and excellent in vitro biocompatibility for biomedical applications. Materials Science and Engineering C, 2013, 33, 3530-3536.	7.3	81
61	Cluster strengthening of Nb-microalloyed ultra-thin cast strip steels produced by the CASTRIP® process. Materials Science & Engineering A: Structural Materials: Properties, Microstructure and Processing, 2013, 568, 88-95.	5.6	26
62	Spatial decomposition of molecular ions within 3D atom probe reconstructions. Ultramicroscopy, 2013, 132, 92-99.	1.9	5
63	The effect of clustering on the mobility of dislocations during aging in Nb-microalloyed strip cast steels: In situ heating TEM observations. Scripta Materialia, 2013, 69, 481-484.	5.2	21
64	High Strength and Retained Ductility Achieved in a Nitrided Strip Cast Nb-Microalloyed Steel. Metallurgical and Materials Transactions A: Physical Metallurgy and Materials Science, 2013, 44, 848-855.	2.2	3
65	The effect of pre-existing defects on the strength and deformation behavior of α-Fe nanopillars. Acta Materialia, 2013, 61, 439-452.	7.9	33
66	An Overview of the Effect of Nb in Strengthening Castrip <sup>®</sup> Steel. Materials Science Forum, 2013, 753, 559-562.	0.3	2
67	In vitro study of the effect of cyclic strains on the dermal fibroblast (GM3384) morphology—Mapping of cell responses to strain field. Medical Engineering and Physics, 2012, 34, 826-831.	1.7	12
68	Enhanced grain refinement of an Al–Mg–Si alloy by high-pressure torsion processing at 100°C. Materials Science & Engineering A: Structural Materials: Properties, Microstructure and Processing, 2012, 552, 415-418.	5.6	43
69	A facile method to in situ formation of hydroxyapatite single crystal architecture for enhanced osteoblast adhesion. Journal of Materials Chemistry, 2012, 22, 19081.	6.7	25
70	Strengthening from Nb-rich clusters in a Nb-microalloyed steel. Scripta Materialia, 2012, 66, 710-713.	5.2	91
71	Overcoming challenges in the study of nitrided microalloyed steels using atom probe. Ultramicroscopy, 2012, 112, 32-38.	1.9	15
72	Insight into the deformation mechanisms of α-Fe at the nanoscale. Scripta Materialia, 2011, 65, 1037-1040.	5.2	20

#	Article	IF	CITATIONS
73	Effect of Nb Microalloying and Hot Rolling on Microstructure and Properties of Ultrathin Cast Strip Steels Produced by the CASTRIP® Process. Metallurgical and Materials Transactions A: Physical Metallurgy and Materials Science, 2011, 42, 2199-2206.	2.2	42
74	Bioactive mesoporeâ€glass microspheres with controllable proteinâ€delivery properties by biomimetic surface modification. Journal of Biomedical Materials Research - Part A, 2010, 95A, 476-485.	4.0	70
75	In vitro studies of cells grown on the superconductor PrOxFeAs. Micron, 2009, 40, 476-479.	2.2	0
76	Nitriding of a Nb-Microalloyed Thin Strip Cast Steel at 525°C. Materials Science Forum, 0, 654-656, 106-109.	0.3	2
77	Effect of Twin Schmid Factor on the Tension Twinning Activities in a Highly Textured Mg-3Al-1Zn. SSRN Electronic Journal, 0, , .	0.4	0
78	Applications of analytical electron microscopy to guide the design of boron carbide. Journal of the American Ceramic Society, 0, , .	3.8	0